



**HAL**  
open science

## Water potential control of turgor-driven tracheid enlargement in Scots pine at its xeric distribution edge

Antoine Cabon, Laura Fernández-de-uña, Guillermo Gea-izquierdo, Frederick Meinzer, David Woodruff, Jordi Martínez-vilalta, Miquel de Caceres

► **To cite this version:**

Antoine Cabon, Laura Fernández-de-uña, Guillermo Gea-izquierdo, Frederick Meinzer, David Woodruff, et al.. Water potential control of turgor-driven tracheid enlargement in Scots pine at its xeric distribution edge. *New Phytologist*, 2020, 225 (1), pp.209-221. 10.1111/nph.16146 . hal-03040768

**HAL Id: hal-03040768**

**<https://hal.inrae.fr/hal-03040768v1>**

Submitted on 17 Jan 2025

**HAL** is a multi-disciplinary open access archive for the deposit and dissemination of scientific research documents, whether they are published or not. The documents may come from teaching and research institutions in France or abroad, or from public or private research centers.

L'archive ouverte pluridisciplinaire **HAL**, est destinée au dépôt et à la diffusion de documents scientifiques de niveau recherche, publiés ou non, émanant des établissements d'enseignement et de recherche français ou étrangers, des laboratoires publics ou privés.

# Water potential control of turgor-driven tracheid enlargement in Scots pine at its xeric distribution edge

Antoine Cabon<sup>1,2</sup> , Laura Fernández-de-Uña<sup>3,4</sup> , Guillermo Gea-Izquierdo<sup>3</sup> , Frederick C. Meinzer<sup>5</sup> , David R. Woodruff<sup>5</sup> , Jordi Martínez-Vilalta<sup>2,6</sup>  and Miquel De Cáceres<sup>1,2</sup> 

<sup>1</sup>Joint Research Unit CTFC - AGROTECNIO, Solsona 25280, Spain; <sup>2</sup>CREAF, Bellaterra (Cerdanyola del Vallès), Catalonia E08193, Spain; <sup>3</sup>INIA-CIFOR, Ctra. La Coruña km. 7.5, Madrid 28040, Spain; <sup>4</sup>UMR Silva, AgroParisTech, Université de Lorraine, INRA, Nancy 54000, France; <sup>5</sup>USDA Forest Service, Pacific Northwest Research Station, Corvallis, OR 97331, USA;

<sup>6</sup>Universitat Autònoma de Barcelona, Bellaterra (Cerdanyola del Vallès), Catalonia E08193, Spain

## Summary

Author for correspondence:

Antoine Cabon

Tel: +34 973 48 16 44

Email: antoine.cabon@ctfc.es

Received: 25 June 2019

Accepted: 19 August 2019

*New Phytologist* (2020) **225**: 209–221

doi: 10.1111/nph.16146

**Key words:** mechanistic model, *Pinus sylvestris*, tracheid enlargement, turgor-driven expansion, water potential, xylogenesis.

- The extent to which water availability can be used to predict the enlargement and final dimensions of xylem conduits remains an open issue.
- We reconstructed the time course of tracheid enlargement in *Pinus sylvestris* trees in central Spain by repeated measurements of tracheid diameter on microcores sampled weekly during a 2 yr period. We analyzed the role of water availability in these dynamics empirically through time-series correlation analysis and mechanistically by building a model that simulates daily tracheid enlargement rate and duration based on Lockhart's equation and water potential as the sole input.
- Tracheid enlargement followed a sigmoid-like time course, which varied intra- and interannually. Our empirical analysis showed that final tracheid diameter was strongly related to water availability during tracheid enlargement. The mechanistic model was calibrated and successfully validated ( $R^2 = 0.92$ ) against the observed tracheid enlargement time course. The model was also able to reproduce the seasonal variations of tracheid enlargement rate, duration and final diameter ( $R^2 = 0.84$ – $0.99$ ).
- Our results support the hypothesis that tracheid enlargement and final dimensions can be modeled based on the direct effect of water potential on turgor-driven cell expansion. We argue that such a mechanism is consistent with other reported patterns of tracheid dimension variation.

## Introduction

Xylem provides woody plants with mechanical support, storage and water transport functions. Wood mechanical and hydraulic properties determine plants' ability to grow in height and to supply the canopy with water to sustain carbon assimilation. Wood properties are in turn largely dependent on the anatomy of xylem conduits (Hacke *et al.*, 2015, 2017). Xylem hydraulic efficiency is extremely sensitive to conduit dimensions as hydraulic conductance increases proportionally to the fourth power of the conduit radius (Tyree & Zimmermann, 2002). On the other hand, conduit dimensions are also associated with xylem hydraulic safety, larger conduits being generally more prone to cavitation during freeze–thaw events (Sperry & Sullivan, 1992; Sperry *et al.*, 1994) as well as to drought-induced embolism (Hacke *et al.*, 2015, 2017). In the case of gymnosperm species, tracheids fulfill both mechanical and hydraulic functions, which further constrains tracheid dimensions (Pittermann *et al.*, 2006).

Xylem conduit dimensions vary greatly along a tree's radial and longitudinal axes, from the intraring scale to the ecoregion scale. Most trees growing under strongly seasonal climates

produce conduits exhibiting periodic diameter variations along the radial axis, resulting in distinct growth rings. In temperate climates, the alternation between wide and thin-walled earlywood conduits and narrow and thick-walled latewood conduits within a ring is a general pattern. There are deviations from this general earlywood–latewood alternation pattern, such as intra-annual density fluctuations, which consist of the inclusion of latewood-like cells within earlywood, or the reverse. Still within the ring but along the longitudinal axis, the universal treetop-to-base widening of xylem conduits (West *et al.*, 1999; Anfodillo *et al.*, 2006; Olson *et al.*, 2014) is associated with a radial increase in xylem conduit dimensions from the pith to the bark as trees grow taller (Fan *et al.*, 2009; Anfodillo *et al.*, 2013). Superimposed on these patterns, climate variability results in year-to-year variation in conduit dimensions (Fonti *et al.*, 2010). Climate can further lead to conduit dimension variations between individual trees, at both the intra- and interspecific levels (Pfautsch *et al.*, 2016). Nevertheless, given that maximum stem height also varies depending on climate, there is some debate regarding the actual source(s) of between-tree conduit diameter variations with climate (Olson *et al.*, 2018).

Understanding the drivers of variations in wood anatomy requires studying the processes at work during wood formation (i.e. xylogenesis). Pioneering studies on conifers established that xylogenesis consists of a sequence of processes occurring in xylem cells successively exiting the cambium until maturation, namely cell division, enlargement, wall thickening and lignification, and programmed cell death (Wodzicki, 1960; Wilson *et al.*, 1966; Skene, 1969). Subsequent technical advances have allowed conifer xylogenesis to be monitored at increasingly higher resolution (Rossi *et al.*, 2006b; Cuny *et al.*, 2013; von Arx & Carrer, 2014), permitting the assessment of the kinetics of the different stages of tracheid differentiation and thereby enabling the investigation of the causes of variation in wood anatomy (Cuny *et al.*, 2014; Rathgeber *et al.*, 2018). Tracheid enlargement kinetics are generally quantified indirectly by identifying them in the enlargement phase using visual criteria (e.g. cell size, birefringence). Enlargement duration is then estimated by dating the entrance and exit of tracheids in this phase. Finally, the tracheid enlargement rate is calculated from estimated enlargement duration and observed final tracheid dimensions at the end of the growing season (Rathgeber *et al.*, 2018). By contrast, there have been comparatively few attempts to directly observe the time course of tracheid size variations between samples, during the period of enlargement (see Antonova *et al.*, 1995; Vaganov *et al.*, 2006). Such observations nonetheless potentially allow estimates of temporally resolved enlargement rates of tracheid cohorts (i.e. tracheids formed at the same moment), which has the potential to help clarify the dynamics of tracheid enlargement and relate it to transient environmental drivers.

Patterns of conduit dimension variations are known to be influenced by environmental cues such as temperature, photoperiod and water availability (Fonti *et al.*, 2010; Begum *et al.*, 2016; Ziaco *et al.*, 2016; Castagneri *et al.*, 2017; Pacheco *et al.*, 2018), as well as internal factors, such as hormonal signaling or sugar availability (Larson, 1960; Funada *et al.*, 2001; Uggla *et al.*, 2001; Winkler & Oberhuber, 2017). More specifically, temperature and water availability have been shown to affect the kinetics of cell differentiation, the interaction of differentiation rates and durations of enlargement, ultimately leading to final tracheid dimensions and cell wall thickness (Balducci *et al.*, 2016; Cuny & Rathgeber, 2016).

Based on this knowledge, models of wood formation have been developed that simulate wood anatomy from environmental factors, including temperature, water availability and day length (Deleuze & Houllier, 1998; Vaganov *et al.*, 2006; Drew & Downes, 2015), while other models describe the relevant physiological determinants, such as sugar availability (Hölttä *et al.*, 2010; Carteni *et al.*, 2018) or hormone gradients (Drew *et al.*, 2010; Hartmann *et al.*, 2017). However, despite these recent breakthroughs, the specific mechanisms of environmental control over xylogenesis in general, and conduit enlargement in particular, still remain unresolved (Vaganov *et al.*, 2011; Rathgeber *et al.*, 2016).

Among the environmental drivers of conduit dimensions, water availability has a pervasive effect, as drier conditions generally lead to the formation of narrower conduits within the ring, from year to year, as well as between individual trees and species

(Deleuze & Houllier, 1998; Fonti *et al.*, 2010; De Micco *et al.*, 2016; Pfautsch *et al.*, 2016). Plant cell expansion is the result of wall relaxation under the action of turgor pressure ( $P$ ) above a yield threshold ( $\gamma_P$ ), which is typically formalized using Lockhart's equation (1965) (see Materials and Methods) and which has been shown to apply to numerous plants and cell types (Green & Cummins, 1974; Cosgrove, 1986). Given the tight relation between cell water status and turgor pressure, Lockhart's equation also explains the high sensitivity of plant cell expansion to water potential (Hsiao, 1973). Experimental work suggests that, in the case of xylem tissue, final conduit dimensions are under similar direct control of water potential (Abe *et al.*, 2003). However, because of the difficulty in directly observing wood cell expansion, there have been few attempts to verify the applicability of Lockhart's equation for explaining variations in conduit expansion and final dimension in response to water potential. Process-based wood formation models have long acknowledged a relationship between conduit enlargement and water availability, among other variables (Deleuze & Houllier, 1998; Fritts *et al.*, 1999). Nevertheless, this link is often represented through empirical relationships, with limited realism and generalization. A family of models has been developed that link stem radial growth to sap flow, based on the application of Lockhart's equation (1965) for cell expansion to whole organ expansion. These models have been successful in predicting subdaily stem diameter variations over a given period of the growing season (Steppe *et al.*, 2006; De Swaef & Steppe, 2010; Hölttä *et al.*, 2010), showing the relevance of plant water relations and turgor-driven cell expansion for modeling wood formation and tree radial growth.

Here we reconstruct the time course of tracheid enlargement in a *Pinus sylvestris* stand near the xeric distribution edge of this species in order to study the dependence of tracheid enlargement and final dimensions on soil water availability. We analyzed the effect of water availability through the quantification of empirical relationships between tracheid diameter (TD) and soil water content (SWC) and by formulating a mechanistic tracheid enlargement model based on Lockhart's equation (1965) for cell expansion, with soil water potential as sole input, which we calibrate and validate against observed tracheid enlargement time courses. Using this mechanistic model, we tested the hypothesis that soil water potential alone can predict tracheid enlargement and final diameter.

## Materials and Methods

### Study site and experimental design

The study site is located in Valsáin (Segovia, central Spain, 40°51'35"N, 4°3'52"W), in the Guadarrama range (facing northwest, 15% slope; 1350 m asl), currently a transition zone between Scots pine (*Pinus sylvestris* L.) and Pyrenean oak (*Quercus pyrenaica* Willd.) dominated stands. The stand is composed of mature pine trees (100 ± 7 yr old) and patches of younger pines (43 ± 4 yr old) and oaks (42 ± 1 yr old). In 2016, optically measured leaf area index (LAI-2200; Li-Cor, Lincoln, NE, USA) was on average 2.3 and 3.1 for old and young pine patches,

respectively. The soil is sandy loam, with 3% organic matter and a bulk density of 0.96 (Díaz-Pinés *et al.*, 2011). Climate is Mediterranean with 728 mm mean annual precipitation, 9.1°C mean annual temperature and a dry period spanning from June to late August. Precipitation and global solar radiation data were obtained for 2013 and 2014 from daily records of nearby weather stations in Segovia (precipitation, 11 km, 1005 m asl) and Navacerrada (solar radiation, 9 km, 1895 m asl) belonging to the Spanish meteorological agency (AEMET) network (Supporting Information Fig. S1). Additionally, daily temperature was recorded on-site during 2013 and 2014 (Fig. S1). Overall, 2013 had approximately average precipitation (808 mm) and temperature (9.2°C), whereas 2014 was wetter (998 mm) and hotter (10.1°C) than usual. The study plot corresponds to the pine control plots of the rainfall-exclusion experiment described in Fernández-de-Uña *et al.* (2017, 2018), where additional methodological details can be found.

### Soil moisture and water potential

Soil water content was monitored hourly during 2013 and 2014 using two sensors at 25 cm depth and three sensors at 50 cm depth (EC-5 Soil Moisture Sensors; Decagon Devices, Pullman, WA, USA) (Fig. S2a). Daily soil water potential ( $\psi_{\text{soil}}$ ; Fig. 1) was calculated from SWC using Van Genuchten's water retention curves, which were parameterized from soil texture, bulk density and organic matter content, following pedotransfer functions described in Tóth *et al.* (2015). Soil texture, bulk density and organic matter fraction were retrieved from a previous study in Valsaín which reported soil properties under three canopy cover types, namely pure oak, pure pine or mixed (Díaz-Pinés *et al.*, 2011). We used the soil properties from the mixed canopy for all calculations. However, to account for the uncertainty surrounding soil properties, we also conducted preliminary analyses

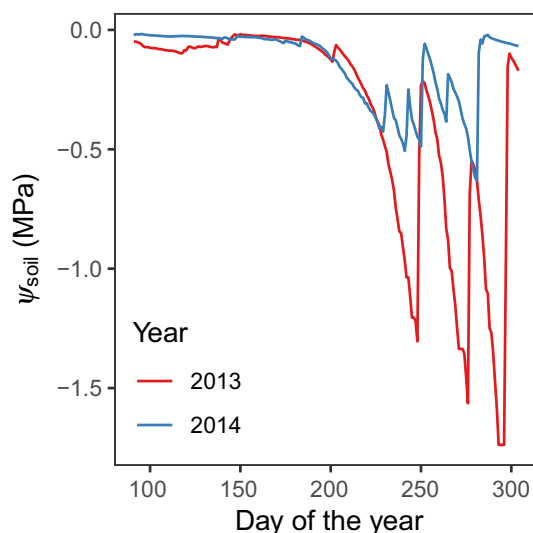


**Fig. 1** Soil water potential ( $\psi_{\text{soil}}$ ) during 2013 and 2014 growing seasons (April–October). Soil water potential was calculated from measured soil moisture using Van Genuchten water retention curves.

using the soil properties from alternative canopy covers. These preliminary analyses showed that the effect of the uncertainty surrounding soil properties on  $\psi_{\text{soil}}$  is of significance only when soil moisture is low (Fig. S2b). To obtain soil water potential values representative of those sensed by pine trees at the study site, soil water potential was then averaged over depth, by weighting each depth contribution by a theoretical root distribution assuming a 1 m rooting depth (Roberts, 1976; Cabon *et al.*, 2018) and a conic root distribution shape. Under this assumption, 95% of the roots are contained in the upper 63 cm of soil. These calculations were done using functions implemented in the R package MEDFATE (De Cáceres *et al.*, 2015).

### Microcore sampling and measurements

A total of 330 microcores were sampled from 12 Scots pines every 7–15 d between April and November, during 2013 and 2014 (six different trees  $\text{yr}^{-1}$ ). Each year, samples were extracted from three trees per size class in order to control for the effect of tree size and age on tracheid development (Rossi *et al.*, 2008) and final tracheid dimensions (Anfodillo *et al.*, 2006). These measures were pooled to provide a more robust characterization of tracheid development patterns (but see Fig. S3 for the tracheid enlargement differences between size classes). Sampled mature trees were, on average,  $103 \pm 5$  yr old,  $22.8 \pm 5.5$  m high and had a diameter at breast height (DBH) of  $48.1 \pm 6.4$  cm, whereas sampled young trees were on average  $41 \pm 4$  yr old,  $13.6 \pm 1.9$  m tall and had a DBH of  $15.4 \pm 3.4$  cm. Microcores were extracted with a Trephor (Rossi *et al.*, 2006a) and stored in a 70% ethanol solution at 4°C. The samples were dehydrated in progressively higher concentrations of ethanol and xylene, embedded in paraffin and cut with a rotary microtome (Fernández-de-Uña *et al.*, 2017). Sections were photographed with a digital camera attached to a microscope ( $\times 100$  magnification) at a resolution of 1.8  $\mu\text{m}$  per pixel.

The radial diameter of the lumen and double cell wall thickness were measured and used to calculate radial TD on all individual cells along three to five files on the current- and previous-year rings using the software DACIA (Hereş, 2013). Cell files were selected so that they were complete (i.e. extending from the beginning of the ring to the cambial zone) and cell boundaries were clearly identifiable. Cells in the cambial zone were distinguished from differentiating cells by their size and shape (Larson, 1994) (see Fig. S4 for an illustration of the measurements). Cell radial dimension measurements were further used to calculate Mork's index of completed rings, following Denne (1989).

### Time course of tracheid enlargement and environmental correlates of final tracheid diameter

There are two main approaches to studying the kinetics of tracheid enlargement (Vaganov *et al.*, 2006). Frequently, tracheid dimensions are measured at the end of the growing season, whereas the timing of tracheid enlargement is estimated by counting the number of tracheids in the enlargement and post-enlargement phases on microcores sampled periodically during

wood formation. The average tracheid enlargement rate is then obtained by dividing final tracheid dimensions by the estimated enlargement duration (Skene, 1969; Wodzicki, 1971; Deslauriers *et al.*, 2003; Rossi *et al.*, 2006b; Cuny *et al.*, 2014). Here we use instead a variation of the ‘instantaneous tracheidogram’ method (Vaganov *et al.*, 2006), which consists of repeated measurements of tracheid dimensions (of all tracheids, i.e. tracheids in both enlargement and post-enlargement stages) through xylogenesis in order to reconstruct the time course of tracheid enlargement for different tracheid cohorts (i.e. tracheids formed around the same time, here defined at the weekly to biweekly scale). The main advantage of this approach lies in that it allows the enlargement rate of each tracheid cohort to be quantified over different time intervals and independently of estimated enlargement duration (details of the protocol are given in Methods S1). This is essential in the case of this study to obtain time-resolved estimates that can be directly compared with model simulations.

In order to visualize the general shape of irreversible tracheid enlargement, we fitted shape constrained additive models (SCAMs) to the measured time course of TD (i.e. the sum of radial lumen diameter and radial cell wall thickness) variations of each tracheid cohort, using the R package SCAM (Pya & Wood, 2015). SCAMs were fitted after a log-transformation of the data and specification of a monotonically increasing smooth function with a gamma distribution of residuals. Weekly tracheid enlargement rate ( $R$ ) was calculated at each time step as the TD increment since the last time step divided by the time difference between the two observations. Tracheid enlargement summary statistics (hereafter referred to as ‘tracheid enlargement features’) were calculated for each weekly tracheid cohort. Maximum tracheid enlargement rate ( $R_{\max}$ ) was defined as the 95% percentile of observed  $R$ . For TD, as this variable follows a saturating function and its distribution is negatively skewed, the 90% percentile of observed TD (rather than 95%) was used to define final tracheid diameter ( $TD_{\max}$ ), thus avoiding overestimation. The cell enlargement duration ( $\Delta t$ ) was defined as the number of days from cell enlargement onset ( $t_1$ ) to reach  $0.9TD_{\max}$  (this threshold is used in order to reduce the uncertainty around the estimate of  $\Delta t$ ). This allowed  $\Delta t$  to be estimated independently from the identification of the different cell differentiation stages. Generalized additive models (Wood, 2011) were finally fitted to tracheid enlargement features in order to describe and visualize their seasonal variations.

Potential direct and lagged empirical monotonic relationships between tracheid final diameter and environmental variables were explored by calculating Spearman’s correlation coefficients ( $\rho$ ) between weekly  $TD_{\max}$  and daily precipitation, temperature, global solar radiation or SWC. These environmental variables were averaged over time periods of 7 d and centered with a lag of  $-120$  to  $54$  d relative to  $t_1$  (54 d being the maximum observed tracheid enlargement duration).

### Tracheid enlargement model

We used Lockhart’s equation (Eqn 1) to model the enlargement of differentiating tracheids as a function of water potential ( $\psi$ ), by expressing the turgor pressure as the difference between  $\psi$  and

osmotic potential ( $\pi$ ) (which is ultimately related to the osmotic pressure difference between the cell and the apoplast):

$$r = \frac{dV}{Vdt} = \begin{cases} \phi(\psi - \pi - \gamma_P), & \psi - \pi > \gamma_P \\ 0, & \psi - \pi \leq \gamma_P \end{cases} \quad \text{Eqn 1}$$

where  $r$  is the relative volume ( $V$ ) increment rate of the cell,  $\phi$  is the cell wall extensibility and  $\gamma_P$  is the turgor pressure threshold to yield expansion. Because we seek to test the extent to which tracheid enlargement and final diameter can be explained by water potential variations alone, we further made the simplifying working assumption that  $\psi$  is the only state variable affecting tracheid enlargement; that is, at any time,  $r$  is a function of  $\psi$  and other variables are either fixed or vary passively as a consequence of cell expansion.

The osmotic potential is the result of the interactions between water molecules and osmolytes within the cell. Assuming that osmolyte fluxes between the cell and the apoplast are negligible, then  $\pi$  varies with cell volume as a result of osmolyte dilution as:

$$\frac{d\pi}{dt} = -nR_m T \frac{dV}{V^2 dt} = -nR_m T \frac{r}{V} \quad \text{Eqn 2}$$

where  $n$  is the osmolyte quantity and  $R_m$  is the gas constant. This assumption implies a decrease of osmolyte concentration with distance to cambium, consistent with observations (Uggla *et al.*, 2001). In addition, concomitant observations of  $\phi$  and  $\gamma_P$  variations during leaf formation in Douglas-fir suggest that  $\gamma_P$  variations are low relative to  $\phi$  (Meinzer *et al.*, 2008). Therefore, we assumed  $\gamma_P$  to be constant in the model. Expansive growth causes cell wall thinning, which is compensated by concomitant wall deposition (Dumais *et al.*, 2006). During late stages of tracheid enlargement, the cell wall becomes thicker and more rigid as wall deposition overcomes thinning (Cosgrove, 2000). We consequently modeled relative variations in  $\phi$  during cell enlargement as the balance between a softening rate, given by the product of  $r$  and a softening constant ( $s$ ), and a constant hardening rate ( $h$ ):

$$\frac{d\phi}{\phi dt} = s \cdot r - h \quad \text{Eqn 3}$$

Finally, as cell expansion is believed to occur mostly at night (but see Mencuccini *et al.*, 2017) when the pressure differential between the plant and the soil is minimal (Pantin *et al.*, 2011; Steppe *et al.*, 2015), we assume here that cell water potential is equal to soil water potential. Note that gravitational effects are assumed negligible at *c.* 1.3 m, the height at which cores were sampled.

Under the assumption that tracheids in the enlargement stage essentially grow radially, then:

$$\frac{dTD}{TDdt} = \frac{dV}{Vdt} = r \quad \text{Eqn 4}$$

Tracheid diameter at a given instant  $t_x$  is then given by integration of the relative enlargement rate (Eqn 5):

$$TD = TD_{t_1} + \exp \int_{t_1}^{t_x} r dt \quad \text{Eqn 5}$$

The tracheid enlargement model (Eqns 1–5) is solved using a finite time discretization approach at the daily scale. Cambial cells had a mean radial diameter of  $8.6 \pm 2.5 \mu\text{m}$  ( $n = 3300$  cells) before exiting the cambial zone. We thus used this value as the initial state of TD in the model ( $TD_{t_1}$ ). The full tracheid enlargement model therefore has five unknown parameters –  $\gamma_P$ ,  $\pi_{t_1}$ ,  $\phi_{t_1}$ ,  $h$  and  $s$  – where  $\pi_{t_1}$  and  $\phi_{t_1}$  are the initial state of the cell osmotic potential and the cell wall extensibility, respectively. The unknown parameters were estimated by model calibration against observed time course of TD variations during 2013, using calculated  $\psi_{\text{soil}}$  as model input. The calibration was conducted by means of minimization of the residual sum of squares using the Nelder–Mead algorithm implemented in the R function ‘optim’ (R Core Team, 2019). Thereafter, the calibrated parameter estimates were compared with values compiled from the literature in order to verify the ability of model calibration to produce realistic parameter estimates. We selected studies in which the parameters were estimated on growing tissue material. However, as we only found one study reporting osmotic potential on growing tissue from a woody species, we also included estimates of osmotic potential concerning nongrowing tissue of pine trees.

The model was first validated by comparing simulated and observed TD time courses in 2014. We then verified the model’s ability to simulate the seasonal variations of tracheid enlargement features in 2013 and 2014 by comparing simulated and observed values of  $TD_{\text{max}}$ ,  $R_{\text{max}}$  and  $\Delta t$ . Finally, to account for uncertainty in model calibration we conducted an analysis of model sensitivity by simulating  $TD_{\text{max}}$ ,  $R_{\text{max}}$  and  $\Delta t$  for the growing season of 2013, using parameter values in the range of those reported in the literature.

## Results

### Observed time course of tracheid enlargement

During the study, tracheid enlargement started in late April (2013, day of year (DOY)  $120 \pm 4$ ; 2014, DOY  $106 \pm 3$ ), ended in mid-August (2013, DOY  $228 \pm 7$ ; 2014, DOY  $234 \pm 9$ ) and the number of tracheids exiting the cambial zone peaked in June (2013, DOY  $169 \pm 5$ ; 2014, DOY  $155 \pm 7$ ). Tracheid enlargement followed a sigmoid-like pattern that was consistent between years and through the growing season (Fig. 2). Cohorts of tracheids formed during the same period of the year exhibited little variability during enlargement, although data were noisier once the saturation plateau was reached. Tracheids formed during the same period of the year but in different years (Fig. 2) or different tree size classes overall had distinct enlargement time courses, but

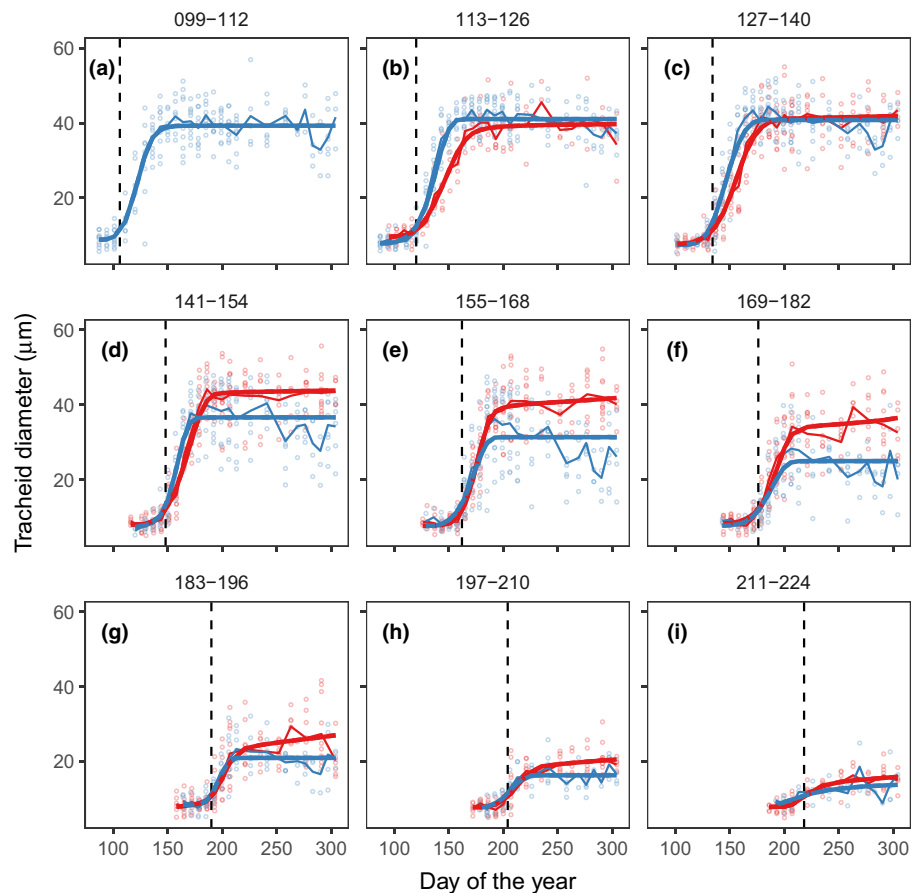


**Fig. 2** Time course of tracheid enlargement during the growing season of 2013 (red) and 2014 (blue). Tracheids are aggregated by cohorts defined based on the date of cell enlargement onset ( $t_1$ ), here at the biweekly scale and plotted in the corresponding panels (a–i; e.g. (a) represents the enlargement time courses of a cohort of tracheids that started enlarging between day of year (DOY) 99 and 112). Vertical dashed lines represent the median tracheid enlargement onset ( $t_1$ ) of each panel. Points are tree-level averages, thin lines are overall averages and curves are fitted shape constrained additive models. On average, the last-formed tracheids entered the enlargement stage on  $DOY 225 \pm 11$ , but tracheids entering the enlargement stage after DOY 224 were not represented because they were too few (1% of the total).

differences tended to disappear for tracheids formed toward the beginning and the end of the growing season (Fig. S3). In 2014, the diameters of tracheids formed in the middle of the growing season showed a marked decrease after having reached their maximum. A small resumed increase in diameter was also observed for tracheids formed during the second half of the 2013 growing season. However, these are most likely artifacts as a result of sampling (see Discussion). After exiting the cambial zone, tracheids grew during  $31 \pm 13$  d on average, at a mean rate of  $0.75 \pm 0.37 \mu\text{m d}^{-1}$ , which yielded an average final diameter of  $31.5 \pm 12.9 \mu\text{m}$ . Tracheid enlargement features varied substantially during the growing season (Figs 2, 3), with  $R_{\text{max}}$  ranging from 0.05 to  $1.19 \mu\text{m d}^{-1}$ ,  $\Delta t$  from 2 to 54 d and  $\text{TD}_{\text{max}}$  from 8.0 to  $45.5 \mu\text{m}$ . According to Mork's index, the earlywood-to-latewood transition corresponded to the tracheids formed around DOY 199 in 2013 (Fig. 2h) and DOY 176 in 2014 (Fig. 2g). Dynamics of  $\text{TD}_{\text{max}}$  and  $R_{\text{max}}$  generally followed a bell-shaped curve skewed towards the end of the growing season, whereas  $\Delta t$  decreased nearly linearly from the beginning to the end of the growing season (Fig. 3).

#### Empirical relationship between tracheid diameter and environmental variables

Calculated Spearman's correlation coefficients between  $\text{TD}_{\text{max}}$  and all environmental variables were highly variable depending on the lag between the two series (Fig. 4). All environmental variables but precipitation reached correlations with significance level  $\alpha < 0.001$ . Precipitation and soil moisture were positively correlated with TD, whereas temperature and solar radiation were mostly negatively correlated. Overall,  $\text{TD}_{\text{max}}$  was best correlated to soil moisture during the period of cell enlargement (lag = 10 d,  $\rho = 0.89$ ). In contrast to soil moisture, temperature and radiation were correlated to  $\text{TD}_{\text{max}}$  at negative lags (scatterplots of the best correlation for each environmental variable are shown in Fig. S5).

#### Tracheid enlargement parameters

Three of the five model parameters, namely the initial osmotic potential ( $\pi_{i1}$ ), the initial cell wall extensibility ( $\phi_{i1}$ ) and the cell wall yield threshold ( $\gamma_P$ ) are frequently measured variables and therefore calibration estimates can be compared with values reported in the literature. In addition,  $\gamma_\psi$  indicates the water potential threshold below which enlargement stops and can be derived from  $\pi_{i1}$  and  $\gamma_P$  ( $\gamma_\psi = \gamma_P + \pi_{i1}$ ). We compiled data from 18 studies in which estimates of one or more enlargement parameters were obtained *in vivo* by direct measurements or indirectly through modeling (Tables 1, S1). The model calibration against observed TD time courses yielded parameters that were consistent with values from the literature (Table 1). Furthermore, calibrated parameters were often closest to estimates corresponding to woody species. Using alternative soil properties to calculate  $\psi_{\text{soil}}$  yielded parameter estimate variations of up to 30% in the case of  $\pi_{i1}$ ,  $\gamma_P$ ,  $\gamma_\psi$  and  $\phi$  but had virtually no effect on the estimates of  $s$  and  $b$  (Table 1).

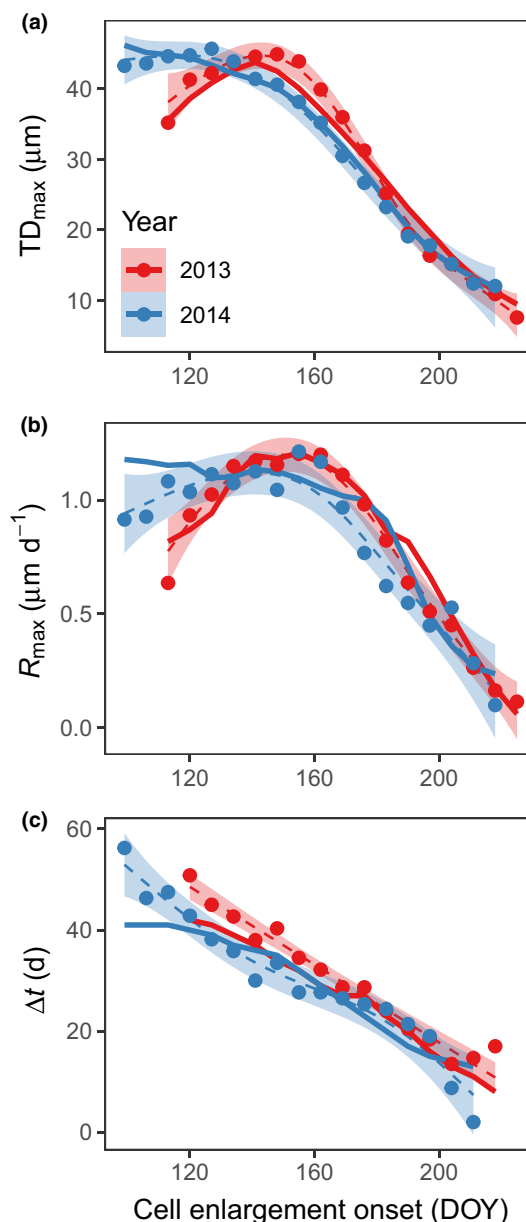


**Fig. 3** Observed (points are means and dashed lines are fitted generalized additive models with 95% confidence intervals as shaded areas) and modeled (solid lines) cell enlargement features as a function of the date of cell enlargement onset for 2013 (red) and 2014 (blue). (a) Final tracheid diameter ( $\text{TD}_{\text{max}}$ ); (b) maximum tracheid enlargement rate ( $R_{\text{max}}$ ); (c) enlargement duration ( $\Delta t$ ).

#### Modeled vs observed tracheid diameter dynamics

All indices showed that model calibration yielded a good fit to observed time course of TD in 2013 (Fig. 5; Table 2; also, see Fig. S6 for details of the fit between observed and simulated TD). The model explained 95% of 2013 TD variability, with very little bias and trend. In 2014, the validation simulations also satisfactorily reproduced the TD variations, although statistics were slightly less good than those of the calibration year: the model still explained 92% of the total variance, with a slightly higher bias and deviation from 1:1 slope in the simulations. Using

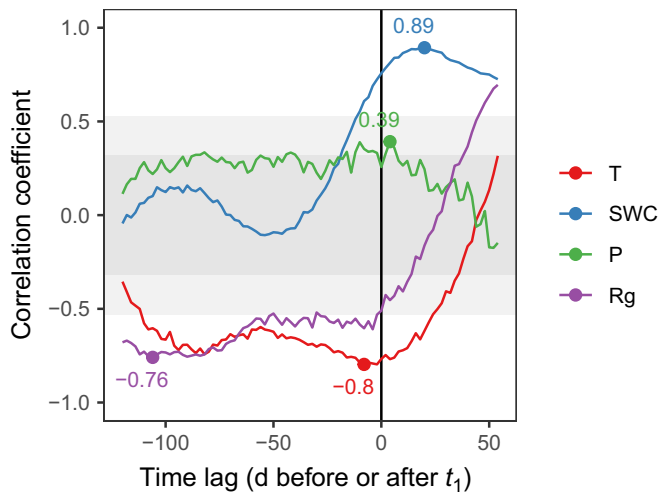


**Fig. 4** Spearman's correlation coefficient ( $\rho$ ) between measured final tracheid diameter ( $TD_{max}$ ; at a weekly resolution, see measured values in Fig. 3a) and environmental variables (T, temperature; SWC, soil water content; P, precipitations; Rg, global solar radiation) averaged following a moving window of 7 d. The lag of the moving window is expressed as the number of d before (negative) or after (positive) the onset of cell enlargement ( $t_1$ ). Points and corresponding values indicate absolute maximum  $\rho$  for each variable. Gray rectangles delimit P-values for which  $P > 0.001$  (light gray) and  $P > 0.05$  (dark gray). When lag = 0 d (vertical solid line), the time window is centered on  $t_1$ . The highest computed positive lag value corresponds to the observed maximum cell enlargement duration (54 d). See scatterplot of the best correlation between  $TD_{max}$  and each environmental variable in Supporting Information Fig. S5.

alternative soil properties to calculate  $\psi_{soil}$  did not affect the model fit, as goodness-of-fit statistics were virtually identical for the different soil textures (Table 2).

### Modeled vs observed tracheid enlargement features

Using the set of parameters calibrated against the time course of tracheid enlargement in 2013, the tracheid enlargement model was able to reproduce the tracheid enlargement features (i.e.  $TD_{max}$ ,  $R_{max}$  and  $\Delta t$ ) for both calibration and validation years (Fig. 3; Table 3). Specifically, modeled  $TD_{max}$  closely fitted observed values, explaining 99% of the  $TD_{max}$  variations along

the ring, with low negative bias for each year. According to the slope of the regression between observations and simulations as well as to the mean absolute error and bias (Table 3; see Fig. S7 for scatter plots of the fit), the fit was even better for the validation year (2014) than the calibration year (2013). In 2013, the model was also good at reproducing the seasonal dynamics of  $R_{max}$  and  $\Delta t$  (explaining *c.* 95% of their variability in both cases). However, in 2014, the model did not perform as well in simulating  $R_{max}$  and  $\Delta t$ , although it still explained *c.* 85% of observed variance in both cases. Overall,  $\Delta t$  was underestimated by 6–12%, whereas  $R_{max}$  was slightly overestimated (*c.* 6%) but the model captured intra- and interannual variations of all tracheid enlargement features.

### Model sensitivity analysis

Predicted  $TD_{max}$  and  $R_{max}$  values for the growing season of 2013 showed high sensitivity to parameter variations, whereas  $\Delta t$  estimates were stable for parameter variations within  $\pm 40\%$ , especially during the second half of the growing season (Fig. 6; supplemental information regarding the sensitivity of the modeled relationship between tracheid growth features and water potential is given in Fig. S8). Model predictions were most sensitive to  $\pi_{t_1}$ , with a 40% increase in this parameter resulting in up to two-fold higher  $TD_{max}$  values and four-fold higher  $R_{max}$  values. Variations of 20% and 40% in  $\gamma_P$  induced little variation in all three tracheid enlargement features, but eight-fold increases in this parameter (thereby matching extreme values reported in the literature; Table 1) did result in large variations for all three tracheid enlargement features, including  $\Delta t$ .  $\gamma_P$  values of *c.* 0.4 MPa (eight-fold increase in  $\gamma_P$ ) yielded predictions of very little tracheid enlargement and a time-window available for enlargement shortened by up to 1 month.

## Discussion

### Measuring tracheid enlargement

The method used here to study tracheid enlargement enabled us to observe the diameter variations of distinct tracheid cohorts

**Table 1** Tracheid enlargement parameters as estimated in this study by model calibration, the values used for the model sensitivity analysis and estimates from the literature.

Parameter	$\pi_{t_1}$ (MPa)	$\gamma_P$ (MPa)	$\gamma_\psi$ (MPa)	$\phi_{t_1}$ (MPa <sup>-1</sup> d <sup>-1</sup> )	s (unitless)	h (d <sup>-1</sup> )
Calibration	-0.79 [-1.01, -0.79]	0.056 [0.056, 0.075]	-0.73 [-0.94, -0.73]	0.13 [0.10, 0.13]	1.8 [1.8, 1.8]	0.043 [0.043, 0.043]
Sensitivity analysis	[-1.1, -0.47]	[0.033, 0.45]		[0.075, 0.18]	[1.1, 2.5]	[0.026, 0.060]
Literature (Woody)	-1.15 (8) [-1.62, -0.55]	0.41 (10) [0.1, 0.78]	-0.67 (6) [-1.4, -0.25]	4.12 (8) [0.020, 17]		
(Herbs)	-1.51 (4) [-1.62, -1.4]	0.11 (2) [0.10, 0.12]	-1.25 (2) [-1.4, -1.1]	0.024 (2) [0.020, 0.028]		
	-0.78 (4) [-1.2, -0.55]	0.45 (8) [0.29, 0.78]	-0.39 (4) [-0.55, -0.25]	5.49 (6) [0.72, 17]		

Calibration estimates are reported for the soil texture under mixed Scots pine-Pyrenean oak canopy as well as minimum and maximum (between square brackets) among estimates obtained using either of the three soil textures to calculate soil water potential ( $\psi_{soil}$ ). Minimum and maximum (between square brackets) are reported for the sensitivity analysis values. Literature estimates are given as averages, sample size (*n*, between parenthesis), minimum and maximum values (between square brackets).  $\pi_{t_1}$ , cell osmotic potential at the onset of cell enlargement, or the osmotic potential at full turgor;  $\gamma_P$ , turgor threshold above which cell enlargement occurs;  $\gamma_\psi$ , plant water potential threshold below which cell turgor is below the yield threshold and  $r = 0$  (i.e.  $\pi_{t_1} + \gamma_P$ );  $\phi$ , cell wall extensibility; *s* and *h*, cell wall softening and hardening constants, respectively. Details on individual parameter literature estimates and the full reference list are given in Supporting Information Table S1.



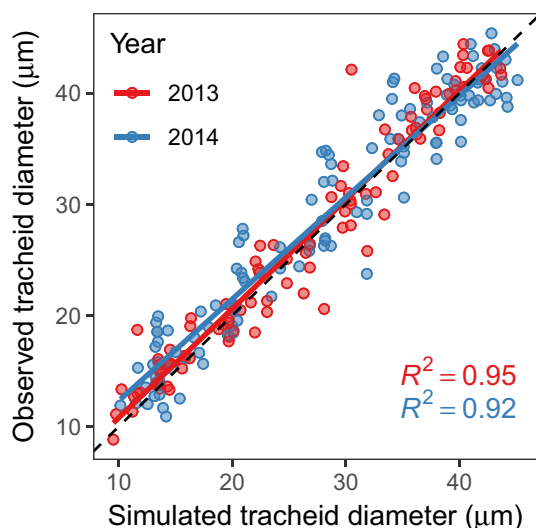


**Fig. 5** Observed vs simulated time course of tracheid enlargement for both calibration (2013) and validation years (2014). Points correspond to observations of tracheid diameter at each sampling date, aggregated by their date of enlargement onset (at the weekly scale). Solid lines correspond to linear regressions between observations and simulations (see summary statistics in Table 2). The black dashed line is the 1 : 1 line.

over time. Consistent with the observations by Sviderskaya and collaborators reported in Vaganov *et al.* (2006), we found that radial tracheid enlargement followed a sigmoid-like pattern. Furthermore, we could show how variations of the general sigmoid pattern between tracheids formed at different dates yielded seasonal and interannual variations in  $TD_{max}$  (Fig. 2). Differences in tracheid enlargement between tree size classes, consistent with the predictable effect of tapering (Fan *et al.*, 2009; Anfodillo *et al.*, 2013), were also observed (Fig. S3).

Compared with more standard xylogenesis kinetics methods (Skene, 1969; Wodzicki, 1971; Deslauriers *et al.*, 2003; Rossi *et al.*, 2006b; Cuny *et al.*, 2014), the method used here allowed us to obtain temporally resolved tracheid enlargement rate estimates, independently of enlargement duration estimates, permitting us to evaluate the impact of transient environmental drivers on tracheid enlargement rate, which is key to validation of our model of tracheid enlargement. Moreover, this method does not rely on the distinction of the differentiation zones of the growing

**Table 2** Statistics of the linear regressions between observed and simulated time course of tracheid enlargement (Fig. 5).

Year	$R^2$	Slope	MAE (%)	Bias (%)
2013	0.95 (0.95)	0.98 (0.97)	7.4 (7.6)	-1.9 (-2.2)
2014	0.92 (0.92)	0.92 (0.91)	9.5 (9.5)	-3.1 (3.4)

The mean absolute error (MAE) is defined as the average of the absolute value of the difference between simulated and observed tracheid diameter divided by the observed diameter. Bias is the average difference between simulated and modeled tracheid diameter divided by the observed tracheid diameter. The statistics values corresponding to simulations using alternative soil texture that yielded the worst statistics are given in parentheses. The overall sample size is 217 ( $n = 99$  in 2013 and  $n = 118$  in 2014).

**Table 3** Statistics of the fit between observed and simulated final tracheid diameter ( $TD_{max}$ ), maximum enlargement rate ( $R_{max}$ ) and enlargement duration ( $\Delta t$ ).

Variable	Year	$R^2$	Slope	MAE (%)	Bias (%)
$TD_{max}$	2013	0.99	1.1	6.1	-1.0
	2014	0.99	1.0	2.9	-0.71
$R_{max}$	2013	0.96	1.0	7.7	3.4
	2014	0.85	0.92	14	8.6
$\Delta t$	2013	0.95	1.0	11	-11
	2014	0.84	1.2	15	-2.8

$R^2$  and the slope correspond to the linear regressions between observation and simulations. The mean absolute error (MAE) is defined as the average of the absolute value of the difference between simulated and observed tracheid diameter divided by the observed diameter. Bias is the average difference between simulated and modeled tracheid diameter divided by the observed tracheid diameter. Overall sample size is 35 ( $n = 17$  in 2013 and  $n = 18$  in 2014).

xylem. This could be an advantage, as distinguishing between the enlargement and wall-thickening zones may be hindered by a certain degree of overlap (Abe *et al.*, 1997; Cosgrove, 2000; Rathgeber *et al.*, 2011; Vaganov *et al.*, 2011 and references therein).

The cited methodological differences could explain why cell enlargement was estimated here to last 30 d on average and up to 54 d, which is about twice what had been previously reported for *P. sylvestris* in continental temperate climates (Wodzicki, 1971; Cuny *et al.*, 2014). Alternatively, these dissimilarities could be a result of phenological differences associated with the location of our study site at the xeric edge of the *P. sylvestris* distribution. Because observed  $TD_{max}$  was nonetheless similar to that observed in the aforementioned studies, the average radial tracheid enlargement rate reported here was about half of that reported in the literature. Cell enlargement duration was found to decrease nearly linearly during the growing season, consistent with previously reported trends (Skene, 1969, 1972; Cuny *et al.*, 2014). Finally, tracheid enlargement rate varied seasonally following a bell-shaped curve skewed towards the end of the growing season. This is consistent with findings of Cuny *et al.* (2014) for *Abies alba* but differs from their results concerning *P. sylvestris*. However, in contrast to enlargement durations, tracheid enlargement rate trends are much less clear and consistent between studies (e.g. Wodzicki, 1971; Dodd & Fox, 1990; Cuny *et al.*, 2014; Balducci *et al.*, 2016). These contrasting results suggest that tracheid enlargement rate is highly variable between species and/or environmental conditions.

In our study, small TD contractions and expansions were sometimes observed once enlargement had apparently reached the saturation plateau. Although these variations could be a result of residual elasticity of the cell wall at a late differentiation stage (Irvine & Grace, 1997), they are more likely biases resulting from the method used here to estimate the time course of TDs (e.g. cell size or cell developmental variability between sampling points). In addition to these trends, the noise surrounding the measures of TD made it difficult to estimate the duration of tracheid enlargement accurately. Despite the potential methodological advantages cited earlier, the fine-scale variations of tracheid

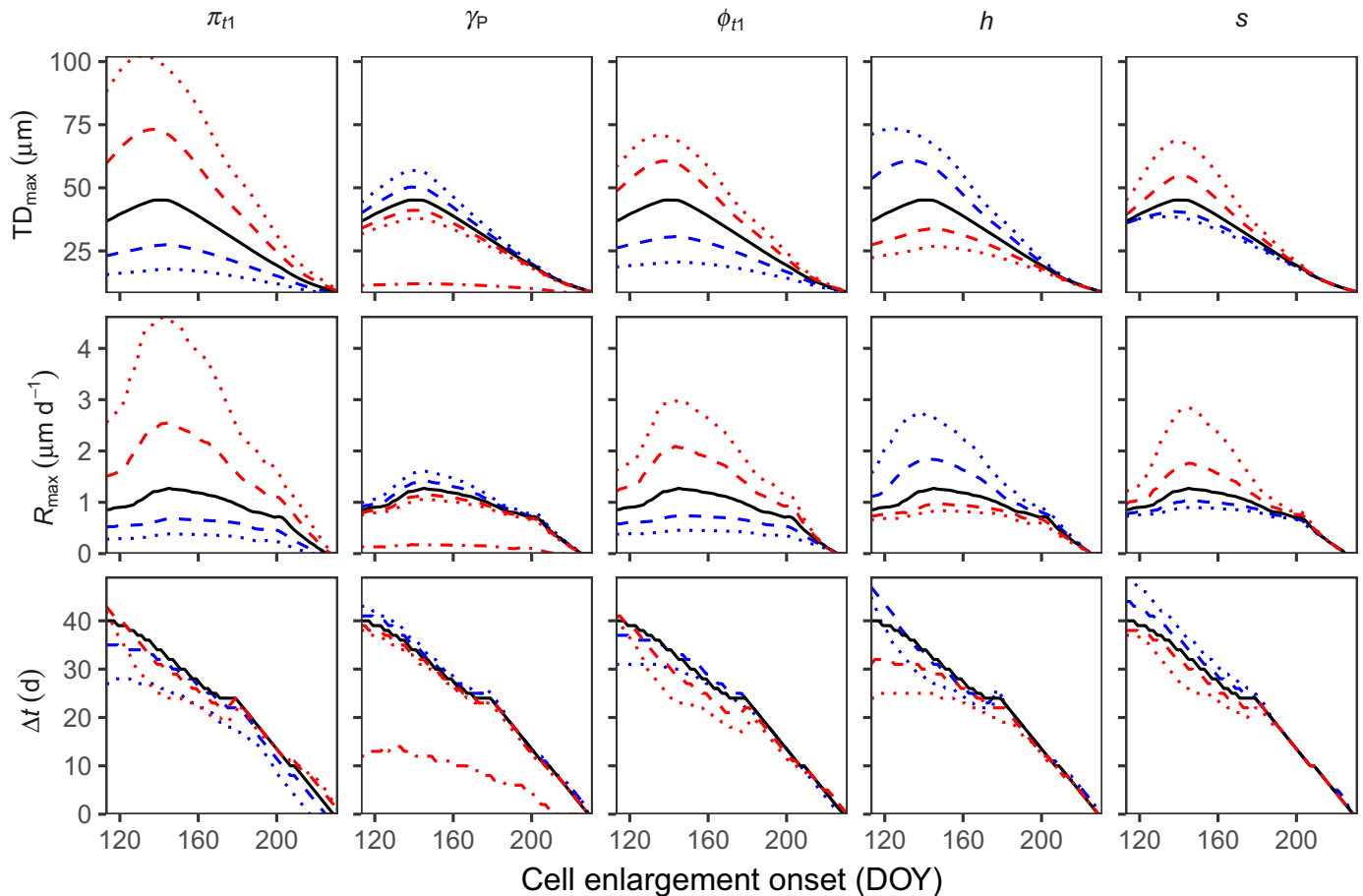


**Fig. 6** Predicted enlargement features ( $TD_{\max}$ , final tracheid diameter;  $R_{\max}$ , maximum tracheid enlargement rate and  $\Delta t$ , tracheid enlargement duration) of cells formed during the growing season of 2013, using the calibrated model parameters (black) as well as parameters increased (red) or decreased (blue) by 20% (dashed lines) or 40% (dotted lines) relative to their calibrated value ( $\pi_{t1}$ , initial osmotic potential;  $\gamma_P$ , yield turgor threshold;  $\phi_{t1}$ , initial cell wall extensibility;  $h$ , cell wall hardening coefficient;  $s$ , cell wall softening coefficient). In the case of  $\gamma_P$ , the model was also run using parameter value multiplied by 8 (dash-dot lines) in order to match the average of values reported in the literature (Table 1).

growth duration as estimated here should thus be interpreted cautiously.

### Water potential control of turgor-driven tracheid enlargement

Final xylem conduit dimensions are known to result from numerous environmental cues, such as temperature and water availability (Fonti *et al.*, 2010). Given the generally high intercorrelation between environmental variables and their temporal autocorrelation, disentangling the actual environmental drivers of xylem conduit enlargement is challenging. Here we found  $TD_{\max}$  to be highly correlated to soil moisture, air temperature and solar radiation (Fig. 4). However, in contrast to temperature and solar radiation, soil moisture was most strongly and positively correlated to TD during the period of tracheid enlargement, when tracheid size is most sensitive to environmental factors (Cuny & Rathgeber, 2016). These results suggest that in the case of our Scots pine stand at the xeric distribution limit of this species, water availability may dominate in explaining the observed TD variations, while the lagged correlation of the other

environmental variables with TD could be explained here by their indirect effect on the water balance (Granier *et al.*, 1999). Whereas temperature or photoperiod are often proposed to explain wood anatomical variations under temperate and cold climates (e.g. Jenkins *et al.*, 1977; Fonti *et al.*, 2013; Björklund *et al.*, 2017), our results are consistent with studies on conifers in water-limited environments (Castagneri *et al.*, 2017, 2018; Belokopytova *et al.*, 2019).

Although other environmental variables (Deleuze & Houllier, 1998; Vaganov *et al.*, 2006; Drew & Downes, 2015) and physiological processes (Drew *et al.*, 2010; Hölttä *et al.*, 2010; Hartmann *et al.*, 2017; Carteni *et al.*, 2018) have proved relevant for modeling wood anatomy, here we focus on water availability in order to assess the hypothesis that water availability alone can explain tracheid enlargement in *P. sylvestris* at our study site. The mechanistic tracheid enlargement model presented here proposes that water potential controls tracheid enlargement through cell turgor. In the model, dynamic feedbacks between cell volume changes and cell osmotic potential and cell wall extensibility further shape the relationship between water potential and cell enlargement. In contrast with other models of wood formation

based on turgor-driven cell expansion (Génard *et al.*, 2001; Steppe *et al.*, 2006; De Swaef & Steppe, 2010; Hölttä *et al.*, 2010), our model does not take into account water and solute fluxes and focuses on the enlargement of individual tracheids, which is modeled in a fully mechanistic manner. Although temporal autocorrelation in the data certainly inflated the fit statistics, model performance was remarkable in most cases. The mechanistic nature of the model, grounded on the widely used and validated Lockhart (1965) equation, and the low number of free parameters reduced the risk of model overfitting. Despite the fact that the exact value of these parameters is uncertain, owing to several potential sources of error regarding model assumptions and input water potential (Table 1), model calibration yielded parameter estimates that were consistent with the literature, especially estimates concerning woody species (Table 1). The model was able to reproduce the observed time course of tracheid enlargement (Fig. 5), regardless of the uncertainty surrounding the input water potential. According to the model, the maximum tracheid enlargement rate is related to water potential at the beginning of cell enlargement, whereas enlargement ceases because of osmotic potential dilution and/or water potential drop. Once tracheid enlargement rate starts to decrease, this trend is further accentuated by the negative feedback of cell wall stiffening. As a result of this hypothesis, a tracheid with low or null enlargement rate rapidly loses its ability to enlarge. Similarly, in their model, Carteni *et al.* (2018) assumed that the cell wall stiffens progressively during tracheid enlargement, but in contrast to the present study, the authors assumed this mechanism to be the primary driver of cell enlargement cessation. Although the changes in cell wall properties were modeled here as a consequence of cell growth rate only, they are also likely to be under metabolic and hormonal control (Schopfer, 2006). This process could thus offer a bridge for incorporating sugar and hormonal signaling in turgor-based modeling of tracheid enlargement (e.g. through modeling variations in the softening (*s*) and hardening (*h*) coefficients).

Finally, the model was also able to accurately reproduce the seasonal variations in tracheid maximum enlargement rate and enlargement duration, as well as the resulting  $TD_{max}$ . The model could simulate the differences in these tracheid enlargement features between 2013 and 2014 as a response to contrasting hydric conditions (Fig. 3). Altogether, these results show that in the case of the studied Scots pine stand, soil water potential is suitable for modeling weekly to annual dynamics of tracheid enlargement. More generally, the results support the model's working assumption, that is, that water potential controls turgor-driven tracheid enlargement. Testing the model under a wider range of water availability is nevertheless an important step in verifying the generality of this finding.

Overall, our model predicts that tracheids formed under drier conditions should be narrower, consistent with observations at the whole-ring level (Fonti *et al.*, 2010). However, this prediction at the individual tracheid level does not necessarily scale up, as drier conditions can also shorten the period of cell production (Balducci *et al.*, 2013; Deslauriers *et al.*, 2016; Fernández-de-Uña *et al.*, 2017, 2018; Vieira *et al.*, 2017), potentially resulting in a

higher proportion of large-diameter tracheids within the growth ring. This may explain why drought is sometimes found to increase mean TD (e.g. Eilmann *et al.*, 2009; Martin-Benito *et al.*, 2013). Further modeling work on tracheid production therefore appears necessary in order to better understand the mechanistic links between climate and wood anatomy.

The simple model formulated here provides a potential mechanism for the occurrence of some important wood anatomical features. Although we acknowledge that the actual environmental drivers may vary depending on climate, our results support the hypothesis that, under water-limiting conditions, the commonly observed decrease in conduit dimensions along the ring, from early- to latewood, is explained by decreasing plant water potential, owing to declining water availability during the growing season (Deleuze & Houllier, 1998; but see Cuny & Rathgeber, 2016). Similarly, the hypothesis of water potential control of turgor-driven tracheid enlargement provides a likely mechanism to explain the occurrence of interannual density fluctuations triggered by temporary drier (wetter) conditions at the beginning (end) of the growing season (De Micco *et al.*, 2016). Furthermore, although angiosperm wood is more complex than gymnosperm wood, the resumption of transpiration and consequent drop in water potential following leaf unfolding after the formation of the first earlywood vessels in ring-porous species (Suzuki *et al.*, 1996; Sass-Klaassen *et al.*, 2011; Kitin & Funada, 2016) could thus induce the steep earlywood-to-latewood decrease in cell dimensions characteristic of these species. Finally, the gradual pressure drop along the hydraulic path (Woodruff *et al.*, 2004; Meinzer *et al.*, 2008) appears to be an adequate candidate to explain the universal tree base-to-top tapering of xylem conduits (Anfodillo *et al.*, 2006, 2012; Olson *et al.*, 2014), as well as limitations to tree height (Koch *et al.*, 2004). Overall, the possibility that the water potential control of turgor-driven conduit enlargement could at least partially explain fundamental patterns of variation in xylem conduit dimensions seems to be a promising area of investigation that deserves further attention.

## Acknowledgements

The authors wish to thank P. Fonti for his numerous and constructive comments on the manuscript. The authors are grateful to the Agencia Estatal de Meteorología (AEMET) for providing daily weather station data.







This research was supported by the Spanish Ministry of Economy and Competitiveness through projects FORESTCAST (CGL2014-59742-C2-2-R) and DRESS (CGL2017-89149-C2-2-R), an FPI pre-doctoral contract to AC (BES-2015-071350) and a Ramon y Cajal fellowship to MDC (RyC-2012-11109) and GGI (RyC-2014-15864). Further support was provided by a Marie Skłodowska-Curie Research and Innovation Staff Exchange (SuFoRun, grant no. 691149) within the European Union's H2020 research and innovation program (H2020-MSCA-RISE-2015). JM-V benefited from an ICREA Academia award. Projects AGL2013-46028R, AGL2010-21153 and AGL2014-61175-JIN from the Spanish Ministry of Economy and Competitiveness and project S2013/MAE-2760 from

Madrid Regional Government funded the establishment of the experimental setup plots and this study's field and laboratory work.

## Author contributions

AC, MDC and JM-V had the original idea of the research question and designed the study. DRW and FCM participated in the theoretical development of the study. LF-d-U and GG-I carried out the field setting design, fieldwork and sample processing. AC wrote the manuscript with contributions from all co-authors.

## ORCID

Antoine Cabon  <https://orcid.org/0000-0001-6426-1726>  
 Miquel De Cáceres  <https://orcid.org/0000-0001-7132-2080>  
 Laura Fernández-de-Uña  <https://orcid.org/0000-0001-8136-2545>  
 Guillermo Gea-Izquierdo  <https://orcid.org/0000-0003-0148-3721>  
 Jordi Martínez-Vilalta  <https://orcid.org/0000-0002-2332-7298>  
 Frederick C. Meinzer  <https://orcid.org/0000-0003-2387-2031>

## References

- Abe H, Funada R, Ohtani J, Fukazawa K. 1997. Changes in the arrangement of cellulose microfibrils associated with the cessation of cell expansion in tracheids. *Trees* 11: 328.
- Abe H, Nakai T, Utsumi Y, Kagawa A. 2003. Temporal water deficit and wood formation in *Cryptomeria japonica*. *Tree Physiology* 23: 859–863.
- Anfodillo T, Carraro V, Carrer M, Fior C, Rossi S. 2006. Convergent tapering of xylem conduits in different woody species. *New Phytologist* 169: 279–290.
- Anfodillo T, Deslauriers A, Menardi R, Tedoldi L, Petit G, Rossi S. 2012. Widening of xylem conduits in a conifer tree depends on the longer time of cell expansion downwards along the stem. *Journal of Experimental Botany* 63: 837–845.
- Anfodillo T, Petit G, Crivellaro A. 2013. Axial conduit widening in woody species: a still neglected anatomical pattern. *IAWA Journal* 34: 352–364.
- Antonova G, Cherkashin V, Stasova V, Varaksina T. 1995. Daily dynamics in xylem cell radial growth of Scots pine (*Pinus sylvestris* L.). *Trees* 10: 24–30.
- von Arx G, Carrer M. 2014. ROXAS – a new tool to build centuries-long tracheid-lumen chronologies in conifers. *Dendrochronologia* 32: 290–293.
- Balducci L, Cuny HE, Rathgeber CBK, Deslauriers A, Giovannelli A, Rossi S. 2016. Compensatory mechanisms mitigate the effect of warming and drought on wood formation. *Plant, Cell & Environment* 39: 1338–1352.
- Balducci L, Deslauriers A, Giovannelli A, Rossi S, Rathgeber CBK. 2013. Effects of temperature and water deficit on cambial activity and woody ring features in *Picea mariana* saplings. *Tree Physiology* 33: 1006–1017.
- Begum S, Kudo K, Matsuoka Y, Nakaba S, Yamagishi Y, Nabeshima E, Rahman MH, Nugroho WD, Oribe Y, Jin HO *et al.* 2016. Localized cooling of stems induces latewood formation and cambial dormancy during seasons of active cambium in conifers. *Annals of Botany* 117: 465–477.
- Belokopytova LV, Babushkina EA, Zhirnova DF, Panyushkina IP, Vaganov EA. 2019. Pine and larch tracheids capture seasonal variations of climatic signal at moisture-limited sites. *Trees - Structure and Function* 33: 227–242.
- Björklund J, Seftigen K, Schweingruber F, Fonti P, von Arx G, Bryukhanova MV, Cuny HE, Carrer M, Castagneri D, Frank DC. 2017. Cell size and wall dimensions drive distinct variability of earlywood and latewood density in Northern Hemisphere conifers. *New Phytologist* 216: 728–740.
- Cabon A, Martínez-Vilalta J, Martínez de Aragón J, Poyatos R, De Cáceres M. 2018. Applying the eco-hydrological equilibrium hypothesis to model root distribution in water-limited forests. *Ecohydrology* 11: e2015.
- Carteni F, Deslauriers A, Rossi S, Morin H, De Micco V, Mazzoleni S, Giannino F. 2018. The physiological mechanisms behind the earlywood-to-latewood transition: a process-based modeling approach. *Frontiers in Plant Science* 9: 1–12.
- Castagneri D, Battipaglia G, von Arx G, Pacheco A, Carrer M. 2018. Tree-ring anatomy and carbon isotope ratio show both direct and legacy effects of climate on bimodal xylem formation in *Pinus pinea* (L. Cernusak, Ed.). *Tree Physiology* 38: 1098–1109.
- Castagneri D, Fonti P, von Arx G, Carrer M. 2017. How does climate influence xylem morphogenesis over the growing season? Insights from long-term intraring anatomy in *Picea abies*. *Annals of Botany* 119: 2011–2020.
- Cosgrove D. 1986. Biophysical control of plant cell growth. *Annual Review of Plant Physiology* 37: 377–405.
- Cosgrove DJ. 2000. Expansive growth of plant cell walls. *Plant Physiology and Biochemistry* 38: 109–124.
- Cuny HE, Rathgeber CBK. 2016. Xylogenesis: coniferous trees of temperate forests are listening to the climate tale during the growing season but only remember the last words!. *Plant Physiology* 171: 306–317.
- Cuny HE, Rathgeber CBK, Frank D, Fonti P, Fournier M. 2014. Kinetics of tracheid development explain conifer tree-ring structure. *New Phytologist* 203: 1231–1241.
- Cuny HE, Rathgeber CBK, Kiessé TS, Hartmann FP, Barbeito I, Fournier M. 2013. Generalized additive models reveal the intrinsic complexity of wood formation dynamics. *Journal of Experimental Botany* 64: 1983–1994.
- De Cáceres M, Martínez-Vilalta J, Coll L, Llorens P, Casals P, Poyatos R, Pausas JG, Brotons L. 2015. Coupling a water balance model with forest inventory data to predict drought stress: the role of forest structural changes vs. climate changes. *Agricultural and Forest Meteorology* 213: 77–90.
- De Micco V, Campelo F, De Luis M, Bräuning A, Grabner M, Battipaglia G, Cherubini P. 2016. Intra-annual density fluctuations in tree rings: how, when, where, and why? *IAWA Journal* 37: 232–259.
- De Swaef T, Steppe K. 2010. Linking stem diameter variations to sap flow, turgor and water potential in tomato. *Functional Plant Biology* 37: 429.
- Deleuze C, Houllier F. 1998. Simple process-based xylem growth model for describing wood microdensitometric profiles. *Journal of Theoretical Biology* 193: 99–113.
- Denne MP. 1989. Definition of latewood according to Mork (1928). *IAWA Journal* 10: 59–62.
- Deslauriers A, Huang J-G, Balducci L, Beaulieu M, Rossi S. 2016. The contribution of carbon and water in modulating wood formation in black spruce saplings. *Plant Physiology* 170: 2072–2084.
- Deslauriers A, Morin H, Bégin Y. 2003. Cellular phenology of annual ring formation of *Abies balsamea* in the Quebec boreal forest (Canada). *Canadian Journal of Forest Research* 33: 190–200.
- Díaz-Pinés E, Rubio A, Van Miegroet H, Montes F, Benito M. 2011. Does tree species composition control soil organic carbon pools in Mediterranean mountain forests? *Forest Ecology and Management* 262: 1895–1904.
- Dodd RS, Fox P. 1990. Kinetics of tracheid differentiation in Douglas-fir. *Annals of Botany* 65: 649–657.
- Drew DM, Downes G. 2015. A model of stem growth and wood formation in *Pinus radiata*. *Trees* 29: 1395–1413.
- Drew DM, Downes GM, Battaglia M. 2010. CAMBIUM, a process-based model of daily xylem development in Eucalyptus. *Journal of Theoretical Biology* 264: 395–406.
- Dumais J, Shaw SL, Steele CR, Long SR, Ray PM. 2006. An anisotropic-viscoplastic model of plant cell morphogenesis by tip growth. *International Journal of Developmental Biology* 50: 209–222.
- Eilmann B, Zweifel R, Buchmann N, Fonti P, Rigling A. 2009. Drought-induced adaptation of the xylem in Scots pine and pubescent oak. *Tree Physiology* 29: 1011–1020.
- Fan Z-X, Cao K-F, Becker P. 2009. Axial and radial variations in xylem anatomy of angiosperm and conifer trees in Yunnan, China. *IAWA Journal* 30: 1–13.

- Fernández-de-Uña L, Aranda I, Rossi S, Fonti P, Cañellas I, Gea-Izquierdo G. 2018. Divergent phenological and leaf gas exchange strategies of two competing tree species drive contrasting responses to drought at their altitudinal boundary. *Tree Physiology* 38: 1152–1165.
- Fernández-de-Uña L, Rossi S, Aranda I, Fonti P, González-González BD, Cañellas I, Gea-Izquierdo G. 2017. Xylem and leaf functional adjustments to drought in *Pinus sylvestris* and *Quercus pyrenaica* at their elevational boundary. *Frontiers in Plant Science* 8: 1–12.
- Fonti P, Bryukhanova MV, Myglan VS, Kiryanov AV, Naumova OV, Vaganov EA. 2013. Temperature-induced responses of xylem structure of *Larix sibirica* (pinaceae) from the Russian Altay. *American Journal of Botany* 100: 1332–1343.
- Fonti P, Von Arx G, García-González I, Eilmann B, Sass-Klaassen U, Gärtner H, Eckstein D. 2010. Studying global change through investigation of the plastic responses of xylem anatomy in tree rings. *New Phytologist* 185: 42–53.
- Fritts HC, Shashkin A, Downes GM. 1999. A simulation model of conifer ring growth and cell structure. In: Wimmer R, Vetter RE eds. *Tree ring analysis: biological, methodological and environmental aspects*. Wallingford, UK: CABI Publishing, 3–32.
- Funada R, Kubo T, Tabuchi M, Sugiyama T, Fushitani M. 2001. Seasonal variations in endogenous indole-3-acetic acid and abscisic acid in the cambial region of *Pinus densiflora* Sieb. et Zucc. Stems in relation to earlywood-latewood transition and cessation of tracheid production. *Holzforschung* 55: 128–134.
- Génard M, Fishman F, Vercambre G, Huguet J-G, Bussi C, Besset J, Habib R. 2001. A biophysical analysis of stem and root diameter variations in woody plants. *Plant Physiology* 126: 188–202.
- Granier A, Bréda N, Biron P, Villette S. 1999. A lumped water balance model to evaluate duration and intensity of drought constraints in forest stands. *Ecological Modelling* 116: 269–283.
- Green PB, Cummins WR. 1974. Growth rate and turgor pressure. *Plant Physiology* 54: 863–869.
- Hacke UG, Lachenbruch B, Pittermann J, Mayr S, Domec J-C, Schulte PJ. 2015. The Hydraulic Architecture of Conifers. In: Hacke U, ed. *Functional and ecological xylem anatomy*. Cham, Switzerland: Springer International Publishing, 39–75.
- Hacke UG, Spicer R, Schreiber SG, Plavcová L. 2017. An ecophysiological and developmental perspective on variation in vessel diameter. *Plant, Cell & Environment* 40: 831–845.
- Hartmann FP, Rathgeber CBK, Fournier M, Moulia B. 2017. Modelling wood formation and structure: power and limits of a morphogenetic gradient in controlling xylem cell proliferation and growth. *Annals of Forest Science* 74: 14.
- Hereş A-M. 2013. *Walking the line between survival and death: drought-induced mortality of Scots pine is associated to distinctive growth and ecophysiological responses*. PhD thesis. Bellaterra, Spain: Autonomous University of Barcelona.
- Hölttä T, Mäkinen H, Nöjd P, Mäkelä A, Nikinmaa E. 2010. A physiological model of softwood cambial growth. *Tree Physiology* 30: 1235–1252.
- Hsiao TC. 1973. Plant responses to water stress. *Annual Review of Plant Physiology* 24: 519–570.
- Irvine J, Grace J. 1997. Continuous measurements of water tensions in the xylem of trees based on the elastic properties of wood. *Planta* 202: 455–461.
- Jenkins PA, Hellmers H, Edge EA, Rook DA, Burdon RD. 1977. Influence of photoperiod on growth and wood formation of *Pinus radiata*. *New Zealand Journal of Forestry Science* 7: 172–191.
- Kitin P, Funada R. 2016. Earlywood vessels in ring-porous trees become functional for water transport after bud burst and before the maturation of the current-year leaves. *LAWA Journal* 37: 315–331.
- Koch GW, Stillet SC, Jennings GM, Davis SD. 2004. The limits to tree height. *Nature* 428: 851–854.
- Larson PR. 1960. A physiological consideration of the springwood summerwood transition in red pine. *Forest Science* 6: 110–122.
- Larson PR. 1994. *The vascular cambium*. Berlin, Heidelberg, Germany: Springer, Berlin Heidelberg.
- Lockhart JA. 1965. An analysis of irreversible plant cell elongation. *Journal of Theoretical Biology* 8: 264–275.
- Martin-Benito D, Beeckman H, Cañellas I. 2013. Influence of drought on tree rings and tracheid features of *Pinus nigra* and *Pinus sylvestris* in a mesic Mediterranean forest. *European Journal of Forest Research* 132: 33–45.
- Meinzer FC, Bond BJ, Karanian JA. 2008. Biophysical constraints on leaf expansion in a tall conifer. *Tree Physiology* 28: 197–206.
- Mencuccini M, Salmon Y, Mitchell P, Hölttä T, Choat B, Meir P, O'Grady A, Tissue D, Zweifel R, Sevanto S *et al.* 2017. An empirical method that separates irreversible stem radial growth from bark water content changes in trees: theory and case studies. *Plant, Cell & Environment* 40: 290–303.
- Olson ME, Anfodillo T, Rosell JA, Petit G, Crivellaro A, Isnard S, León-Gómez C, Alvarado-Cárdenas LO, Castorena M. 2014. Universal hydraulics of the flowering plants: vessel diameter scales with stem length across angiosperm lineages, habits and climates. *Ecology Letters* 17: 988–997.
- Olson ME, Soriano D, Rosell JA, Anfodillo T, Donoghue MJ, Edwards EJ, León-Gómez C, Dawson T, Camarero Martínez JJ, Castorena M *et al.* 2018. Plant height and hydraulic vulnerability to drought and cold. *Proceedings of the National Academy of Sciences, USA* 115: 7551–7556.
- Pacheco A, Camarero JJ, Carrer M. 2018. Shifts of irrigation in Aleppo pine under semi-arid conditions reveal uncoupled growth and carbon storage and legacy effects on wood anatomy. *Agricultural and Forest Meteorology* 253–254: 225–232.
- Pantin F, Simonneau T, Rolland G, Dauzat M, Muller B. 2011. Control of leaf expansion: a developmental switch from metabolics to hydraulics. *Plant Physiology* 156: 803–815.
- Pfautsch S, Harbusch M, Wesolowski A, Smith R, Macfarlane C, Tjoelker MG, Reich PB, Adams MA. 2016. Climate determines vascular traits in the ecologically diverse genus *Eucalyptus*. *Ecology Letters* 19: 240–248.
- Pittermann J, Sperry JS, Wheeler JK, Hacke UG, Sikkema EH. 2006. Mechanical reinforcement of tracheids compromises the hydraulic efficiency of conifer xylem. *Plant, Cell & Environment* 29: 1618–1628.
- Pya N, Wood SN. 2015. Shape constrained additive models. *Statistics and Computing* 25: 543–559.
- R Core Team. 2019. *R: A Language and Environment for Statistical Computing (v.3.5.3)*. Vienna, Austria.
- Rathgeber CBK, Cuny HE, Fonti P. 2016. Biological basis of tree-ring formation: a crash course. *Frontiers in Plant Science* 7: 1–7.
- Rathgeber CBK, Longuetaud F, Mothe F, Cuny H, Le Moguédec G. 2011. Phenology of wood formation: data processing, analysis and visualisation using R (package CAVIAR). *Dendrochronologia* 29: 139–149.
- Rathgeber CBK, Santenoise P, Cuny HE. 2018. CAVIAR: an R package for checking, displaying and processing wood-formation-monitoring data (R Tognetti, Ed.). *Tree Physiology* 38: 1246–1260.
- Roberts J. 1976. A study of root distribution and growth in a *Pinus sylvestris* L. (Scots pine) plantation in East Anglia. *Plant and Soil* 44: 607–621.
- Rossi S, Anfodillo T, Menardi R. 2006a. Trephor: a new tool for sampling microcores from tree stems. *LAWA Journal* 27: 89–97.
- Rossi S, Deslauriers A, Anfodillo T. 2006b. Assessment of cambial activity and xylogenesis by microsampling tree species: an example at the Alpine timberline. *LAWA Journal* 27: 383–394.
- Rossi S, Deslauriers A, Anfodillo T, Carrer M. 2008. Age-dependent xylogenesis in timberline conifers. *New Phytologist* 177: 199–208.
- Sass-Klaassen U, Sabajo CR, den Ouden J. 2011. Vessel formation in relation to leaf phenology in pedunculate oak and European ash. *Dendrochronologia* 29: 171–175.
- Schopfer P. 2006. Biomechanics of plant growth. *American Journal of Botany* 93: 1415–1425.
- Skene DS. 1969. The period of time taken by cambial derivatives to grow and differentiate into tracheids in *Pinus radiata*. *Annals of Botany* 33: 253–262.
- Skene DS. 1972. The kinetics of tracheid development in *Tsuga canadensis* Carr. and its relation to tree vigour. *Annals of Botany* 36: 179–187.
- Sperry JS, Nichols KL, Sullivan JEM, Eastlack SE. 1994. Xylem embolism in ring-porous, diffuse-porous, and coniferous trees of northern Utah and interior Alaska. *Ecology* 75: 1736–1752.
- Sperry JS, Sullivan JEM. 1992. Xylem embolism in response to freeze-thaw cycles and water stress in ring-porous, diffuse-porous, and conifer species. *Plant Physiology* 100: 605–613.

- Steppe K, De Pauw DJW, Lemeur R, Vanrolleghem PA. 2006. A mathematical model linking tree sap flow dynamics to daily stem diameter fluctuations and radial stem growth. *Tree Physiology* 26: 257–273.
- Steppe K, Sterck F, Deslauriers A. 2015. Diel growth dynamics in tree stems: linking anatomy and ecophysiology. *Trends in Plant Science* 20: 335–343.
- Suzuki H, Yoda K, Suzuki M. 1996. Phenological comparison of the onset of vessel formation between ring-porous and diffuse-porous deciduous trees in a Japanese temperate forest. *IAWA Journal* 17: 431–444.
- Tóth B, Weynants M, Nemes A, Makó A, Bilas G, Tóth G. 2015. New generation of hydraulic pedotransfer functions for Europe. *European Journal of Soil Science* 66: 226–238.
- Tyree MT, Zimmermann MH. 2002. Hydraulic architecture of whole plants and plant performance. *Xylem structure and the ascent of sap*. Berlin, Heidelberg, Germany: Springer, 175–214.
- Uggla C, Magel E, Moritz T, Sundberg B. 2001. Function and dynamics of auxin and carbohydrates during earlywood/latewood transition in Scots pine. *Plant Physiology* 125: 2029–2039.
- Vaganov EA, Anchukaitis KJ, Evans MN. 2011. How well understood are the processes that create dendroclimatic records? A mechanistic model of the climatic control on conifer tree-ring growth dynamics *Dendroclimatology* 2: 37–75.
- Vaganov EA, Hughes MK, Shashkin AV. 2006. Growth dynamics of conifer tree rings. In: Caldwell MM, Heldmaier G, Jackson RB, Lange OL, Mooney HA, Schulze E-D, Sommer U eds. *Ecological studies*. Berlin/Heidelberg, Germany: Springer, 1–354.
- Vieira J, Nabais C, Rossi S, Carvalho A, Freitas H, Campelo F. 2017. Rain exclusion affects cambial activity in adult maritime pines. *Agricultural and Forest Meteorology* 237–238: 303–310.
- West GB, Brown JH, Enquist BJ. 1999. A general model for the structure and allometry of plant vascular systems. *Nature* 400: 664–667.
- Wilson BF, Wodzicki TJ, Zahner R. 1966. Differentiation of cambial derivatives: proposed terminology. *Forest Science* 12: 438–440.
- Winkler A, Oberhuber W. 2017. Cambial response of Norway spruce to modified carbon availability by phloem girdling. *Tree Physiology* 37: 1527–1535.
- Wodzicki T. 1960. Investigation on the kind of *Larix polonica* Rac. wood formed under various photoperiodic conditions. I. Plants growing in natural conditions. *Acta Societatis Botanicorum Poloniae* 29: 714–730.
- Wodzicki TJ. 1971. Mechanism of xylem differentiation in *Pinus silvestris* L. *Journal of Experimental Botany* 22: 670–687.
- Wood SN. 2011. Fast stable restricted maximum likelihood and marginal likelihood estimation of semiparametric generalized linear models. *Journal of the Royal Statistical Society: Series B (Statistical Methodology)* 73: 3–36.
- Woodruff DR, Bond BJ, Meinzer FC. 2004. Does turgor limit growth in tall trees? *Plant, Cell & Environment* 27: 229–236.
- Ziaco E, Biondi F, Heinrich I. 2016. Wood cellular dendroclimatology: testing new proxies in great basin bristlecone pine. *Frontiers in Plant Science* 7: 1602.

## Supporting Information

Additional Supporting Information may be found online in the Supporting Information section at the end of the article.

**Fig. S1** Weekly averages of temperature, solar radiation and precipitation records.

**Fig. S2** Daily soil water content measurements and calculated soil water potential.

**Fig. S3** Tree size effect on the time course of tracheid enlargement.

**Fig. S4** Image of measurements conducted on slides obtained from microcores.

**Fig. S5** Scatter plot of empirical relationship between  $TD_{max}$  and environmental variables.

**Fig. S6** Observed and simulated time course of tracheid enlargement.

**Fig. S7** Scatter plot of observed vs simulated features of tracheid enlargement.

**Fig. S8** Sensitivity of the modeled relationship between tracheid enlargement and water potential to varying parameters.

**Methods S1** Reconstructing the time course of tracheid enlargement from repeated microcore sampling.

**Table S1** Cell enlargement parameters as estimated in this study by model calibration and estimates from the literature.

Please note: Wiley Blackwell are not responsible for the content or functionality of any Supporting Information supplied by the authors. Any queries (other than missing material) should be directed to the *New Phytologist* Central Office.